PYSICS OF THE ICE AGE CYCLE

W. Richard Peltier
Department of Physics
60 St. George St.
University of Toronto
Toronto, Ontario
Canada M5S 1A7

During the last half of the Pleistocene epoch, beginning roughly 900,000 yrs ago, the variability evidenced in the climate system has been dominated by the 100 kyr ice age cycle first recognized by Broecker and Van Donk (1970). The sequence of events during this time has been markedly improved recently by employing the Milankovitch hypothesis of the origin of ice ages to refine our knowledge of their chronology! Various physical models of this long timescale climate oscillation have been proposed that may be distinguished either as "wet", in the sense that they rely in large part upon internal forcing due to variation in the strength of the thermohaline circulation (e.g. Broecker and Denton, 1989) or as "dry", in which case they posit a secondary role for the oceans. Following a brief review of developments in the area of ice age chronology, I will discuss recent and ongoing attempts to resolve the issue as to whether the ice age cycle is primarily a "wet" or a "dry" phenomenon.

Introduction

Since its first recognition by Broecker and Van Donk (1970) in $\delta^{18}0$ data from deep sea sedimentary cores, the issue of the explanation of the 100 kyr ice-age-cycle that has dominated climate system variability for the last 900 kyr of Pleistocene time has remained outstanding. Although the seminal paper by Hays et al. (1976) has often been misconstrued as establishing the validity of the astronomical theory of Milankovitch (e.g. 1941), in fact nothing could be further from the truth. What this analysis did establish was that the spectral signature of the summertime seasonal orbital insolation anomaly was indeed impressed indelibly upon deep sea

NATO ASI Series, Vol. I 22
Long-Term Climatic Variations
Edited by J.-C. Duplessy and M.-T. Spyridakis

$\delta^{18}0$ records. These records, which are understood to be proxy for continental ice volume (Shackleton, 1967), reveal statistically significant concentrations of spectral power at the period of 41 kyr that is contained within the summertime seasonal insolation anomaly due to the change in orbital obliquity, and at 19 kyr, 21 kyr and 23 kyr due to the contribution to insolation change by eccentricity modulation of the precessional cycle. However, Milankovitch's theory posited a direct, which is to say linear, link between variations in summertime insolation and variations in continental ice volume. If this theory were correct then all significant variance in deep sea $\delta^{18}0$ records would be found at these orbitally significant periods. In fact more than 60% of the variance in typical deep sea $\delta^{18}0$ records over the last 700 kyr of earth history is associated with the 100 kyr ice age cycle mentioned above and there is no significant power at this period in the insolation anomaly time series that Milankovitch believed to be responsible for inducing the ice ages (e.g. Hyde and Peltier 1987). Understanding the ice age cycle therefore clearly obliges us to identify the nonlinear interaction(s) within the climate system that are responsible for transforming the applied orbital insolation forcing (which has no significant 100 kyr component) into the observed ice volume response whose spectrum is dominated by the low frequency 100 kyr oscillation.

In order to provide focus for the discussion to follow, I show on Figure 1a the $\delta^{18}0$ time series from the highest resolution deep sea sedimentary record that is presently available. This record, from ODP Site 677 in the Panama Basin off the west coast of South America, has been extensively discussed from the perspective of chronology by Shackleton et al. (1990). Also shown beneath the top plate on this Figure are a number of different statistical characterizations (discussed in the figure caption) of the change of the statistical character of the record with time from about 2 Myr ago (the beginning of the record) to the present. Clearly evident, even by visual inspection, is the fact that the last 900 kyr of $\delta^{18}0$ (ice volume) variability has been dominated by the 100 kyr ice-age-cycle in which ice volume rises slowly to a maximum over a period of about 90 kyr and then "terminates" in an episode of rapid decrease that occurs on a time scale of about 10 kyr. Prior to about 900 kyr ago, however, the 100 kyr cycle is essentially absent from the record. A time dependent spectrum of the original time series (Figure 2), often referred to as a digital sonogram, demonstrates that in the earliest Myr of time all significant variance in the $\delta^{18}0$ time series is found in the spectral lines expected on the basis of the astronomical theory whereas, following 900 kyr BP (before present), the time series is dominated

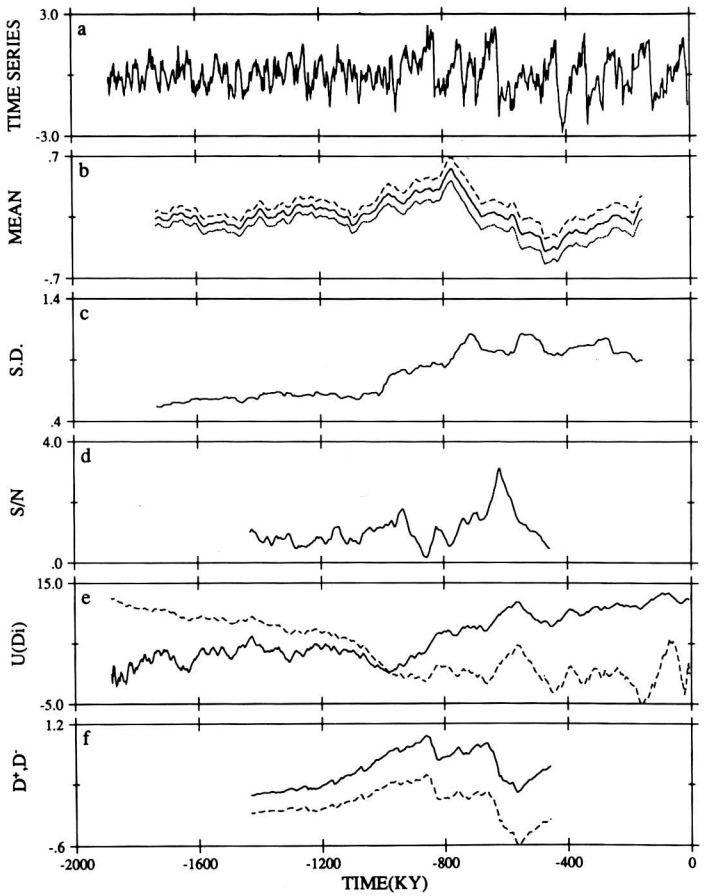

Figure 1. Statistical analysis of ODP site 677 $\delta^{18}0$ record with the depth age curve corresponding to model II discussed below. (a) Time series. (b) Running mean of the time series shown in (a) with segment length of 300 kyr. (c) Changing standard deviation of the time series shown in (a) computed for a segment length of 300 kyr. (d) Signal over noise ratio averaged over a range of segment lengths of 300 to 450 kyr. (The confidence level is 99%). (e) Mann-Kendall rank statistic, U(Di), for forward (solid) and retrograde (dashed) time series. (f) Test for jump in variance, D^+ (solid line) and D^- (dashed line), averaged over the same segment lengths as in (d).

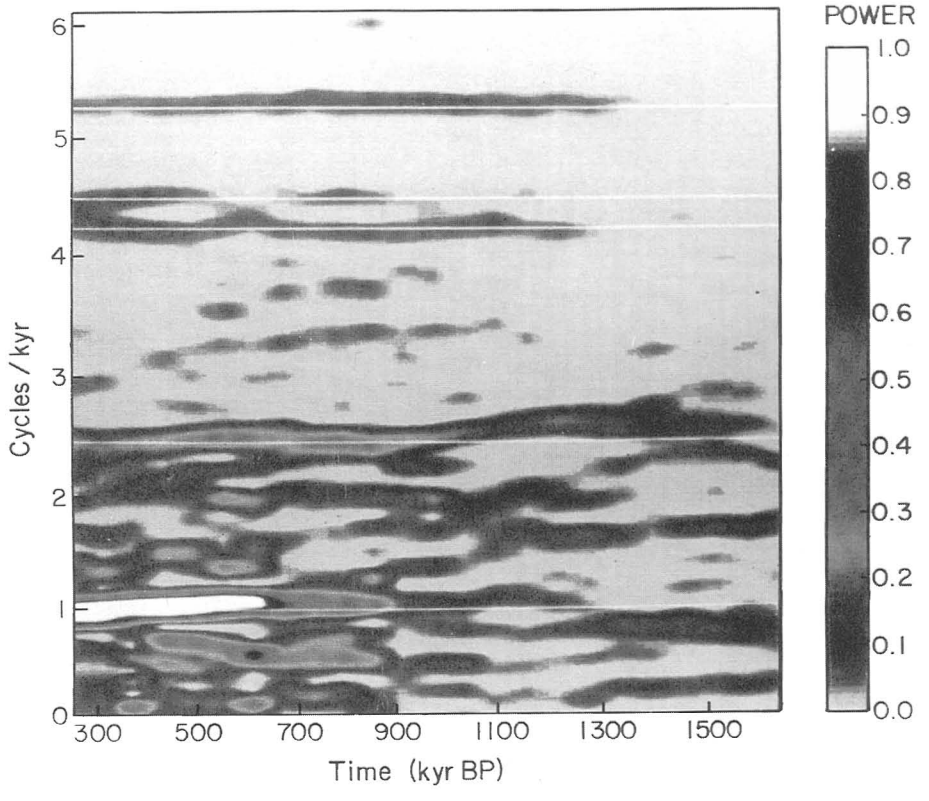

Figure 2. Digital sonogram of the ODP 677 time series shown in Figure 1. This time dependent power spectrum has been computed using a running time window 500 kyr in length. The horizontal (white) reference lines are at the orbitally significant periods of 19, 21, 23, 41 and 100 kyr. Note that the strong 100 kyr component of climate system variability is not evident until about 900 kyr BP.

by the "unexplained" 100 kyr ice-age-cycle. In the remainder of this paper I will review recent theoretical attempts to explain the ice age cycle, following a brief review of the issue as to how an appropriately accurate chronology may be established for deep sea sedimentary $\delta^{18}0$ data such as those shown in Figure 1.

Ice-Age Chronology

In the previously referred to seminal analysis of Hays et al. (1976) which first conclusively demonstrated, through spectral analysis of appropriate $\delta^{18}0$ time series from deep sea cores, that the periodicities predicted by the Milankovitch theory were indeed evident in these ice volume proxy records, the time scale for each record was fixed by appeal to magneto-stratigraphy. What one did was to find the depth in the core at which the induced magnetization in the sedimentary grains reversed direction. This depth, which is quite easily observed in cores taken from sufficiently high geographic latitude, was taken to correspond to an age of 730,000 ± 10,000 yrs on the basis of the previously well established chronology of magnetic field reversals produced on the basis of age and magnetic measurements in land based sequences of volcanic rocks (e.g. Cox et al. 1963). Assuming a constant sedimentation rate, unique to each core, one could thereby construct a linear map from depth to time and thereby convert the $\delta^{18}0$ vs. depth data into a $\delta^{18}0$ vs. time series such as the one shown on Figure 1a. This practise essentially reached is apogee with publication of the so called SPECMAP timescale by Imbrie et al. (1984). This timescale was believed to be accurate for ages slightly beyond the age of the Brunhes-Matuyama boundary at 730,000 ± 10,000 yrs and was based upon a stacked sequence of records. In the later analysis of individual sedimentary cores sufficiently long to reach further back in time, (e.g. DSDP 607, Raymo et al. 1990) this timescale was simply transferred to the cores by the correlation of appropriate control points and thereafter extended to greater depth.

With the availability of the very high resolution $\delta^{18}0$ data set from the ODP 677 site (Shackleton and Hall, 1989), for which no magnetostratographic control was available, an alternate method for establishing an appropriate timescale suggested itself to the author. This was essentially an extension of the method employed to refine the youngest part of the SPECMAP scale by Martinson et al. (1987) who adjusted the timescale in a relatively short sedimentary record so as to achieve maximum/shallowest time domain coherence between an appropriate

orbital insolation time series and the $\delta^{18}0$ signal in the deep sea core by bandpassing both the insolation record and the $\delta^{18}0$ record through a filter with a 41 kyr passband and then adjusting the timescale in the deep sea core so as to achieve maximum time domain coherence between the two filtered time series. Since the $\delta^{18}0$ record from the ODP 677 core was of sufficiently high resolution that the triplet of lines in the above described eccentricity - precession band should also be well resolved, a somewhat more sophisticated version of the Martinson approach became a viable objective method of determining an age model for this core.

This new method, results of which were first reported by the author at a meeting on the Milankovitch theory that was held at the Lamont-Doherty Observatory in 1988, consisted of iteratively refining the timescale through the following sequence of steps.

1. A first guess timescale was assumed to correspond to the SPECMAP scale in the shallowest portion of the record and was extended to the deepest level by assuming constant sedimentation rate.
2. The resulting time series was bandpassed through a filter with a central period of 41 kyr. This bandpass filter is shown in the power spectrum diagram of Figure 3 in terms of its spectral response characteristics.
3. The summertime seasonal insolation time series for an assumed control latitude, say 55°N, was next bandpass filtered through the same 41 kyr filter described in 2.
4. The timescale employed in step 2 was then adjusted so as to achieve best time domain coherence between the 41 kyr signals in the filtered $\delta^{18}0$ and insolation time series in the top most part of the record.
5. Using the updated timescale from step 4 on which to represent the $\delta^{18}0$ data, the ODP 677 record was next bandpassed through a filter, also shown on Figure 3 in terms of its spectral response characteristics, with a central period of 21 kyr.
6. The same caloric summertime seasonal insolation signal employed in 3 was next bandpassed through the same 21 kyr filter applied to the $\delta^{18}0$ record in step 5.
7. The revised timescale developed by obliquity tuning in step 4 was then further adjusted over the same top-most-part of the record so as to achieve an equally high quality time domain fit to the eccentricity-precession signal as that achieved in step 4 at the obliquity period.
8. The iterative sequence of steps 4-7 was then repeated, moving ever further down the core in each successive repetition of the sequence.

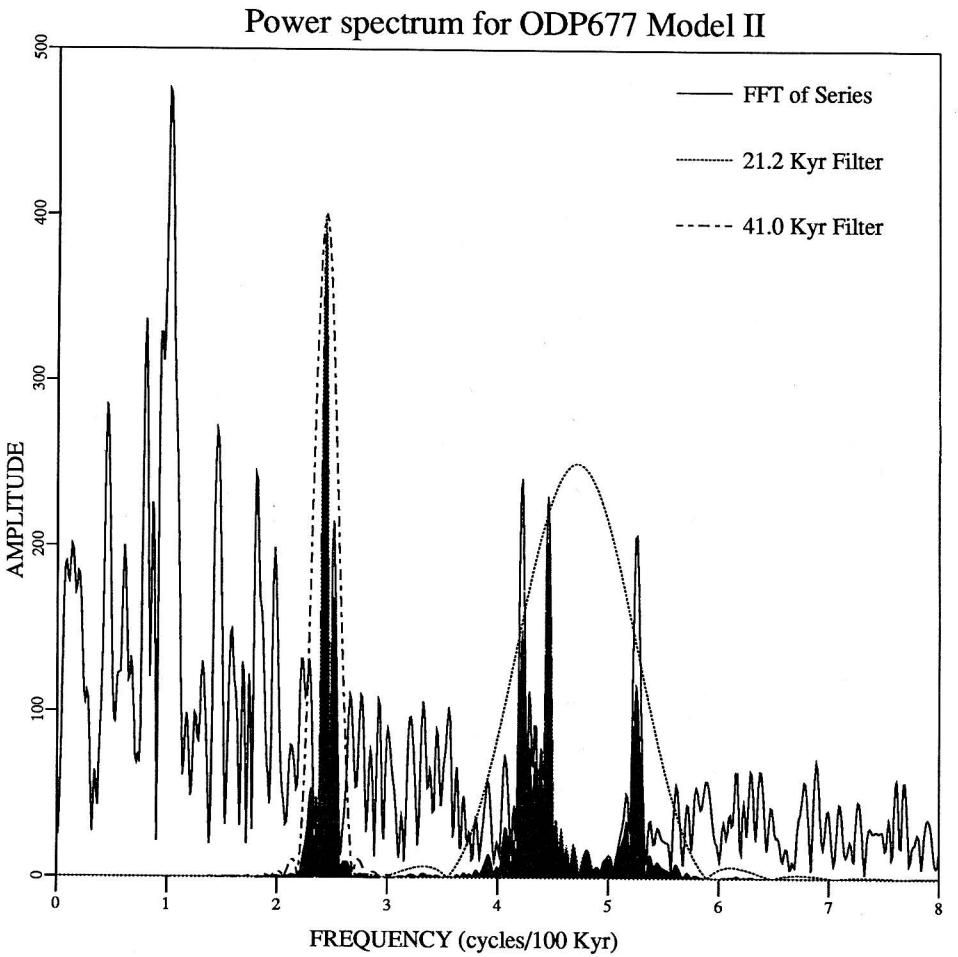

Figure 3. Power spectrum of the entire ODP 677 record using the chronostratigraphy corresponding to age model II on Figure 4. The dash-dotted and dotted curves represent the spectral transfer functions of the bandpass filters used to tune the chronostratigraphy in the obliquity and eccentricity-precession bands respectively. The solid black regions represent the spectrum of ODP 677 seen through these filters.

Figure 4 compares four different timescales for the ODP 677 record. The first, labelled I, is the timescale obtained by tuning the record solely to the 41 kyr obliquity period while that labelled II, the preferred timescale, is obtained by tuning both to obliquity and to the eccentricity-

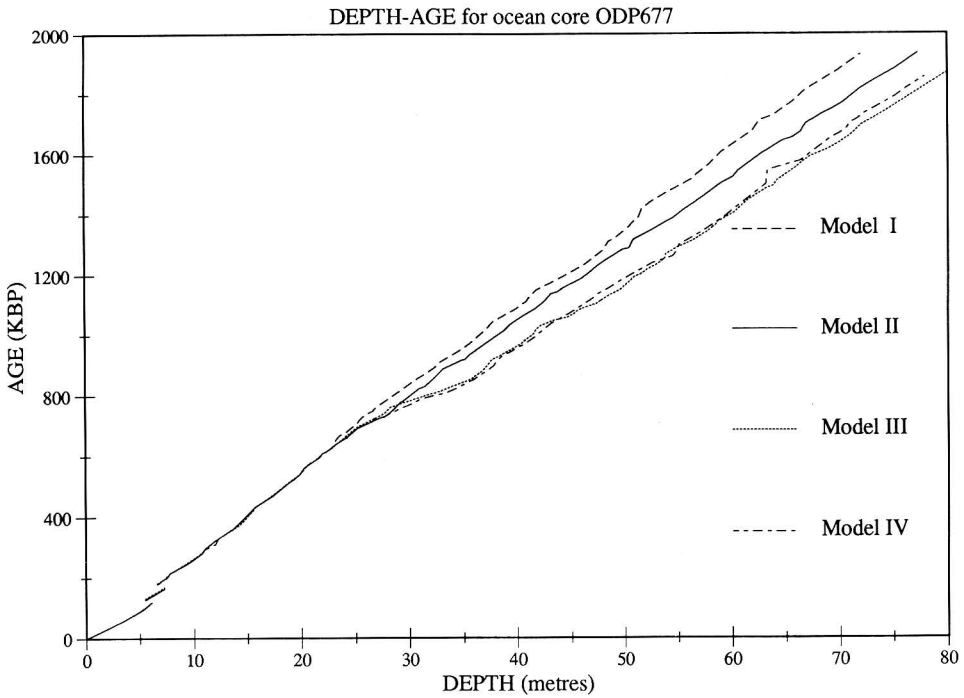

Figure 4. Four age models for ODP 677. Model I is the result obtained by tuning only in the obliquity band. Model II is iteratively tuned to produce optimum time domain coherence in both the obliquity and eccentricity-precession bands. Model III was obtained by Shackleton (personal communication) by transferring the chronostratigraphy from the DSDP 607 core to ODP 677. Model IV is a variant on model III.

precession signal. This timescale is characterized by an almost constant sedimentation rate. In comparison, the timescale labelled III is the timescale delivered by transferring the timescale from DSDP core 607 to the ODP 607 core by correlating "like" features. This timescale and its near relative labelled IV is clearly characterized by a marked change in sedimentation rate near 700 kyr B.P. The "quality" of the constant sedimentation rate timescale labelled II may be assessed by inspection of the time domain coherence between the obliquity and eccentricity precession signals in the $\delta^{18}0$ time series and in the orbital insolation time series. These comparisons are shown in Figures 5 and 6 respectively. Although it cannot be seen as

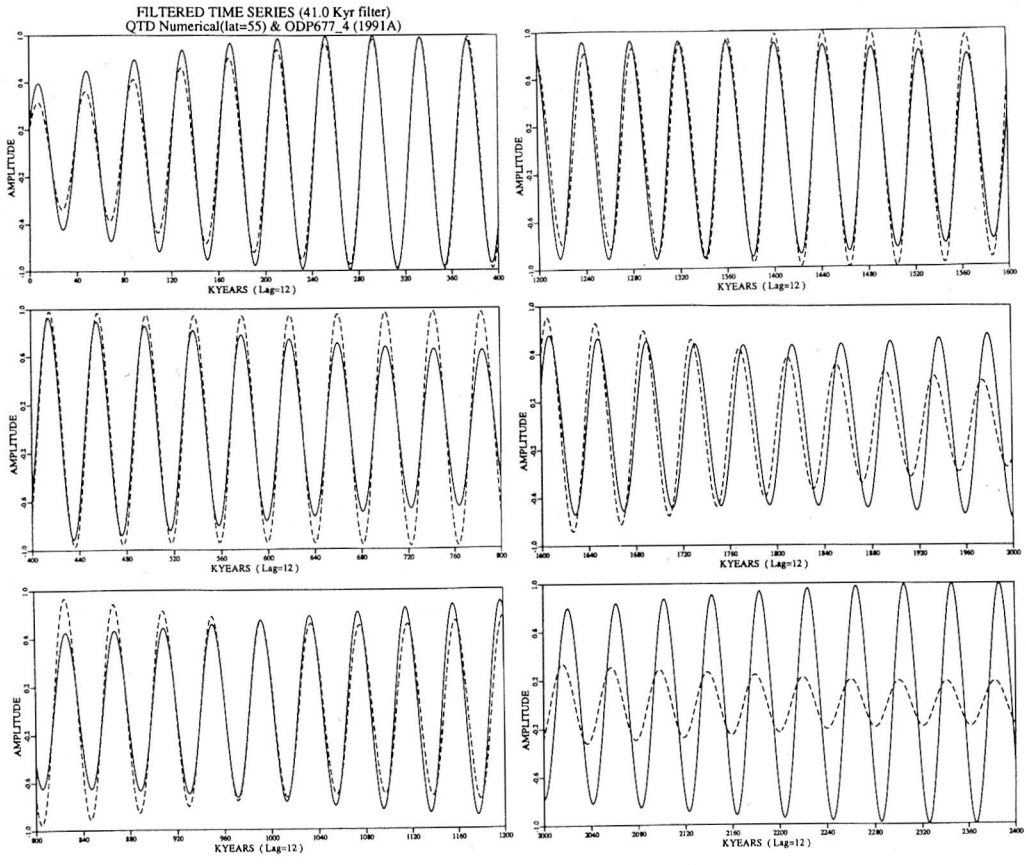

Figure 5. The 55°N insolation signal according to the Quinn et al. (1991) astronomical reconstruction bandpassed through the 41 kyr filter (solid) compared to the ODP 677 record on age model II (dashed) bandpassed through the same filter.

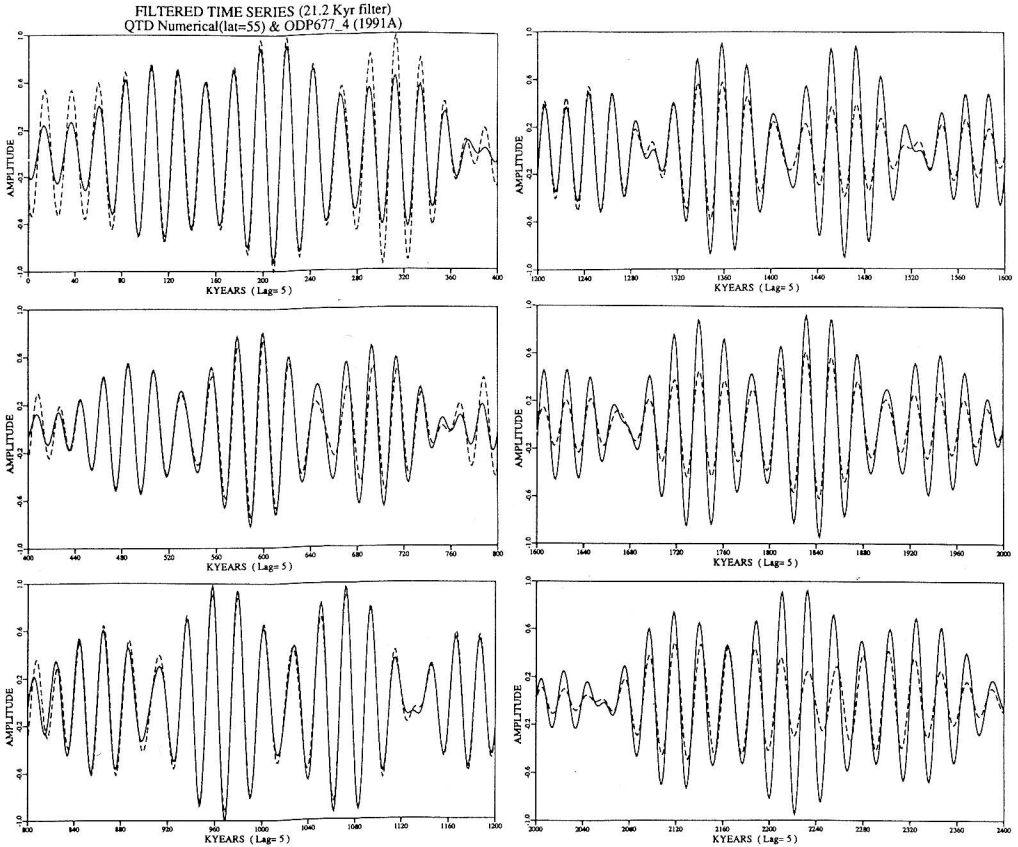

Figure 6. Same as for Figure 5 but comparing the astronomical signal with ODP 677 in the eccentricity-precession band.

remarkable that it is possible to achieve the nice time domain coherence between insolation and $\delta^{18}0$ at the period of the 41 kyr "singlet" (Figure 5) it is in fact remarkable that the characteristic beating in time due to the interference between the three component lines in the eccentricity - precession "multiplet" can be so accurately recovered in the $\delta^{18}0$ data by an appropriate choice of timescale. Inspection of Figure 4 furthermore shows that the timescale that delivers this extraordinary time domain coherence between $\delta^{18}0$ and insolation is one which deviates minimally from a constant sedimentation rate timescale. Comparing this timescale with that transferred from the DSDP 607 (Atlantic) core of Ruddiman and Raymo (1988) it is clear that the latter implies the existence of a marked change in sedimentation rate between 700 and 800 kyr BP.

If one accepts the new almost constant sedimentation rate timescale labelled II on Figure 4, however, then one is obliged to face the objection that this would imply that the previously determined radiometric age for the Brunhes-Matuyama reversal is too young by about 7%, i.e. somewhat more than an obliquity cycle. This was first pointed out in the analysis presented by Shackleton et al. (1990) based upon very much less detailed tuning of the ODP 677 timescale than discussed above. Although there was some initial reluctance in the community to accept this possibility, Baksi et al. (1993) have very recently demonstrated, by employing the very accurate $^{39}Ar/^{40}Ar$ step heating procedure, that in fact the previously accepted age of the Brunhes-Matuyama boundary was indeed too young by precisely the 7% suggested on the basis of the above described Milankovitch tuning procedure. This must be seen as an extraordinary demonstration of the power of the Milankovitch insight that orbitally induced changes of summer seasonal insolation could be responsible for causing substantial changes of continental ice volume. Even though the astronomical theory of Milankovitch cannot explain the strong variability of ice volume at the 100 kyr period that has dominated climate system history for the last 900 kyr, the orbital signal is nevertheless clearly evident in $\delta^{18}0$ records throughout the Pleistocene epoch. Theoretical efforts to explain how this signal is transformed to create the 100 kyr oscillation will be discussed in the following subsections.

A model of the 100 kyr cycle and the mid-Pleistocene transition

In attempting to understand the 100 kyr cycle it is clearly important to understand not only how

a 100 kyr response might be engendered in the climate system by an insolation forcing that contains essentially no power at this period, but it is also equally important to seek to understand why the 100 kyr component of the response was essentially absent prior to 900 kyr ago even though the insolation signal in this earlier period differed insignificantly from that in more recent time. In a recent attempt to address these questions, DeBlonde and Peltier (1991) have further developed the model originally introduced by Peltier (1982) and employed in a sequence of initial experiments by Hyde and Peltier (1985, 1987). This model couples the three basic ingredients illustrated schematically in Figure 7, namely a circumpolar ice sheet whose thickness is a function of latitude only, the viscously delayed response of the earth to the loading of its surface by this ice sheet, and the orbital insolation forcing of Milankovitch that is assumed to enter the system via a proportional latitudinal motion of the so-called equilibrium line. The latter separates the region of accumulation from the region of ablation.

The mathematical realization of this model consists of the vertically integrated continuity equation for ice mass, in the from:

$$\frac{\partial H}{\partial t} = \frac{\lambda}{a \sin\theta} \frac{\partial}{\partial \theta} \left[\frac{\sin\theta H^5}{a} \left(\frac{\partial h}{\partial \theta} \right)^2 \frac{\partial h}{\partial \theta} \right] + G(\theta, t) \tag{1}$$

in which $\lambda = C (\rho_i g)^3/5$ with C a constant that depends upon the microphysical properties of ice, ρ_i is ice density and g is the surface gravitational acceleration. The dependent variables in (1), H and h, are respectively ice thickness and the height of the surface of the ice sheet above mean sea level. H is therefore decomposed in the sum $H(\theta,t) = h(\theta,t) + h'(\theta,t)$ as on Figure 7 in which h' is the depression of the solid surface of the earth below its equilibrium level due to the weight of the ice load. The latter deflection is in part elastic and in part viscous and its evolution with time may be accurately calculated using the detailed theory of glacial isostatic adjustment developed in Peltier (1974, 1976, 1985). This theory delivers the evolution equation for the field $h'(\theta,t)$ required to complete (1) as

$$\frac{\partial h'(\theta,t)}{\partial t} = \frac{3\rho_i}{\rho_a} \left\{ \sum_l P_l \int P_l' \sin\theta' \left[\sum_j -r_j^l s_j^l e^{-s_j^l t} D_j^l(\theta',t) + \sum_j r_j^l H(\theta',t) \right] d\theta' \right.$$

$$\left. + \sum_l P_l \int P_l' \sin\theta' \, q_l^E \frac{\partial H(\theta',t)}{\partial t} \, d\theta' \right\} \tag{2}$$

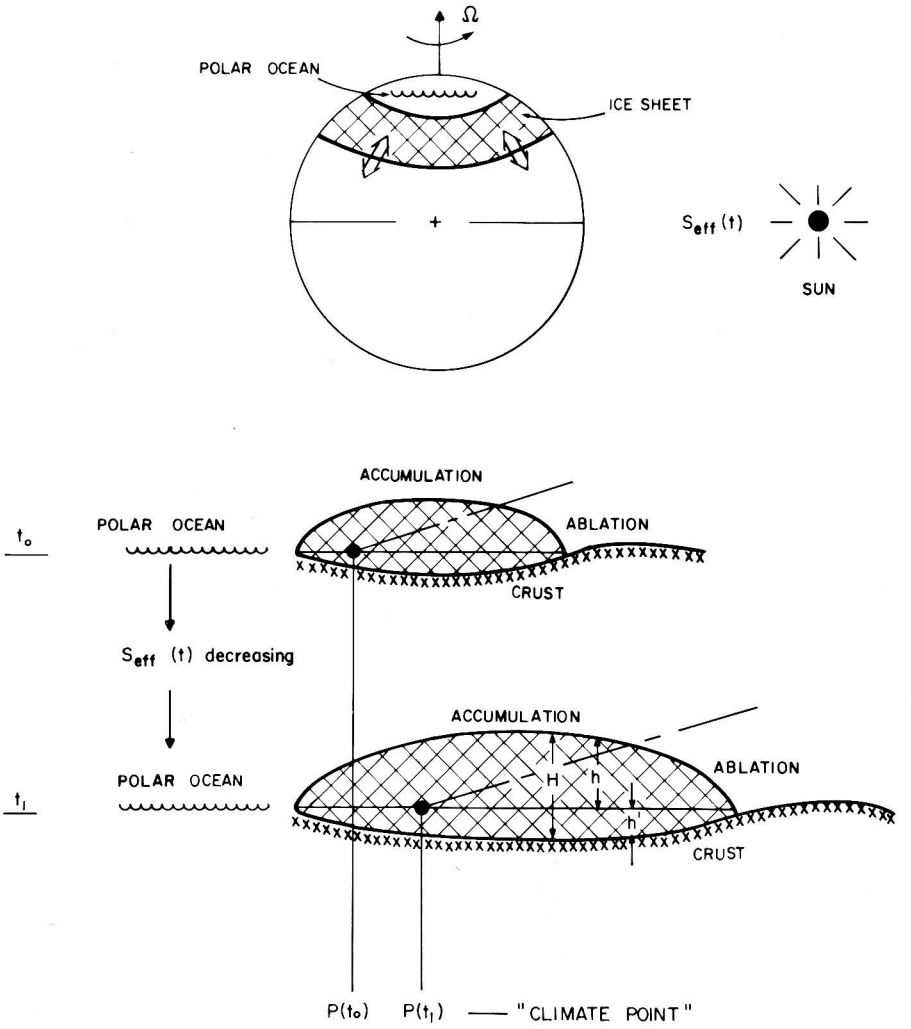

Figure 7. Schematic diagram indicating the physical components of the one dimensional nonlinear model of the ice-ages that has been designed to explain the appearance of the 100 kyr cycle in the ODP 677 record.

in which

$$D_j^{\ell}(\theta',t) = \int_o^t H(\theta',t')\, e^{s_j^{\ell} t'}\, dt'$$

so that

$$\frac{\partial D_j^{\ell}}{\partial t} = H(\theta',t)\, e^{s_j^{\ell} t} \tag{3}$$

In order to integrate the dynamical system embodied in equations (1)-(3) one first steps (3) forward in time to update the D_j^{ℓ}. In the second step (2) is integrated forward to a obtain a new field $h'(\theta,t)$. Finally the nonlinear diffusion equation (1) is integrated forward to update $H(\theta)$. In (2) the P_{ℓ} are conventional Legendre polynomials, ρ_a is the average density of the earth, the r_j^{ℓ} and s_j^{ℓ} are the amplitudes and inverse relaxation times of the discrete set of normal modes of viscous gravitational relaxation that are required to characterize the viscous part of the glacial isostatic adjustment process (Peltier 1974, 1976, 1985) and the q_{ℓ} are the elastic surface load Love numbers of degree ℓ that appear in this theory.

In (1) the mathematical form employed for the accumulation function $G(\theta,t)$ is simply (e.g. Oerlemans 1980, Pollard 1982):

$$G(x,t) = \begin{cases} a(h-E) - b(h-E)^2, & for\ (h-E) \le 1500\,m \\ 0.56\,m\,yr^{-1}, & for\ (h-E) > 1500\,m \end{cases} \tag{4}$$

where E is the so-called equilibrium line that tilts upwards to the south as on the sketch in Figure 7. North of the point of intersection of this line with the surface of the ice sheet is the accumulation zone. The ablation zone is to the south. On the equilibrium line itself where h=E, G≡0. Following Milankovitch (1941) we assume that positive anomalies in caloric summer seasonal insolation ΔQ induce a rise in the equilibrium line and thus an increase in the scale of the ablation zone and thus a diminution of ice mass. The position of the equilibrium line is computed according to the representation (with x=sinθ):

$$E(x,t) = E_o - s(x - x_o) + k\Delta Q(t) \tag{5}$$

The anomaly ΔQ(t) should be computed using the results of Quinn et al. (1991) but I shall

illustrate the response of the above described model using the 55°N forcing from Berger (1978). The constants a,b and s,k in (4) and (5) are listed in DeBlonde and Peltier (1991). In order to obtain an adequate simulation of the ODP 607 record shown on Figure 1 we are obliged to further augment the above structure with an additional ad hoc feedback loop, the possible origins of which I shall discuss below. This feedback loop amounts to an acceleration of the ablation process whenever the model embodied in the above equations delivers an ablation rate that exceeds some critical value. As in Pollard (1983) we define an instantaneous melting rate as:

$$\dot{M} = (-3.0 \times 10^{-7}\ m^{-1})\ \frac{dC}{dt} \tag{6}$$

in which C is the instantaneous cross-sectional area of the ice sheet in Figure 7. When $\dot{M}$ exceeds some critical value, 12 cm yr^{-1} is employed here ($\dot{M}$ being expressed in terms of an equivalent rate of sea level rise), then it is sharply increased to 20 cm yr^{-1}. This is equivalent to a raising of the equilibrium line by 500-1000 m and thus to a temperature rise of 3-6°C, assuming an atmospheric lapse rate of 6.5°C km^{-1} (see DeBlonde and Peltier 1991 for more detailed discussion). As we will see, the nature of the response that the model delivers to the applied insolation forcing depends critically upon whether or not this additional feedback loop is engaged or disengaged.

An example of the response of the model to the Milankovitch input for 55°N latitude is shown in Figure 8a along with the same statistical characterizations of the time series as were shown on Figure 1 in connection with the discussion the ODP 677 record. Visual inspection of this synthetic ice volume record demonstrates that it has the same qualitative features as the deep sea $\delta^{18}0$ record from the Panama basin. In order to achieve this high quality fit to the observations what has been done is to "switch-on" the above described additional feedback loop at 900 kyr BP with simultaneous changes in E_o and k of 250 m and 11 m $(W\ m^{-2})^{-1}$. When this additional feedback is turned off as it is in the first half of the simulated record then the response to orbital forcing is just as predicted by Milankovitch with significant power only at the periods present in the incoming insolation. Once the feedback has been turned-on, however, the dominant response is at the 100 kyr period that is characteristic of the ice-age cycle. The issue then clearly arises as to what this ad hoc positive feedback in the model should be taken to represent. In the model of Pollard (1983) it was imagined to be due to calving into proglacial lakes during the

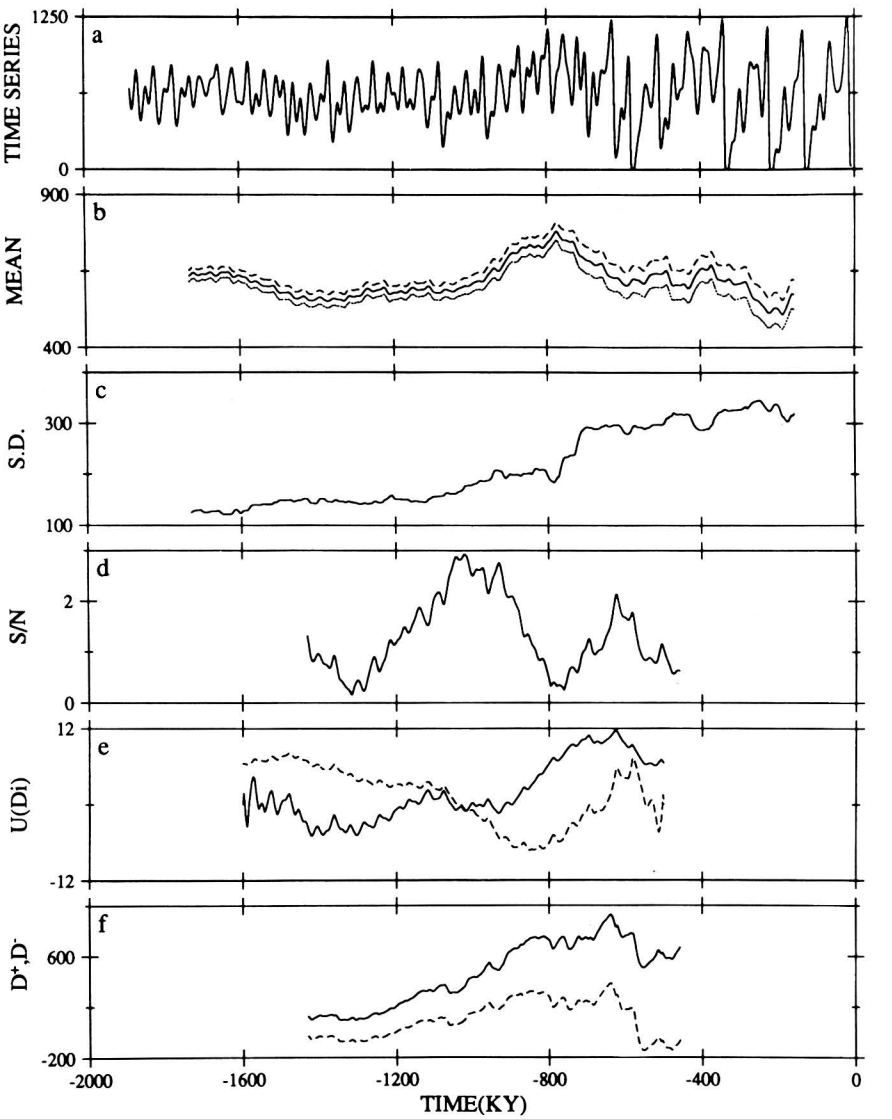

Figure 8. Same as for Figure 1 but the time series in plate (a) is a simulation of the ODP 677 record based upon the integration of the one dimensional non-linear model described in the text.

retreat of a large (e.g. Laurentide) ice sheet. The heat capacities of such lakes are so small, however, that it is hard to imagine how they could provide the forcing required. Other candidates are of course possible to imagine and of these it will suffice to mention two only, one "dry", the other "wet". In the category of "dry" feedbacks the most plausible seems to me to be that associated with terrigenous dust (e.g. De Angelis et al. 1987) since it is now well established both on the basis of ice core records and deep sea sedimentary cores that each of the strong 100 kyr pulses of ice sheet advance and retreat were characterized by extremely high dust levels in the full glacial phase of the cycle that preceded the termination. Peltier and Marshall (1993) have recently tested this hypothesis and found it to be tenable. This is clearly a "dry" mechanism. Of the possible "wet" mechanisms, I believe that the idea of a marine based instability of the Laurentide ice margin such as was undoubtedly responsible for the recently discovered Heinrich events (e.g. Heinrich 1988) is the most deserving of further attention.

One way in which one might hope to better understand which of these mechanisms (or some other) is actually responsible for the 100 kyr cycle is simply to make the above described model more physically realistic without adding any further physical processes. This is the idea to which I turn in the next subsection.

Multiple ice sheets in a global energy balance model: the origin of terminations

The one dimensional model described in the last subsection clearly has a number of unrealistic characteristics. Foremost amongst these is that, lacking realistic geography, it is unable to distinguish the west European ice complex from the North American complex. The ice thickness distributions within these two main continental ice sheets, as recently deduced on the basis of the inversion of postglacial relative sea level data by Tushingham and Peltier (1991), are shown on Figure 9. There is very little evidence to support the notion that there was significant ice in Eastern Siberia and this fact may on the surface appear to be unexpected. In proceeding, as I shall do in the present section, to add detail to the model of the last Section, my goal will be in part to explain this apparent paradox and to demonstrate how far we can in fact go in explaining the detailed thickness distribution for glacial maximum shown in Figure 9. An equally important goal, however, is to discover whether or not, with a slightly more complex model describing the interaction of the same physical processes previously considered, we might discover a more

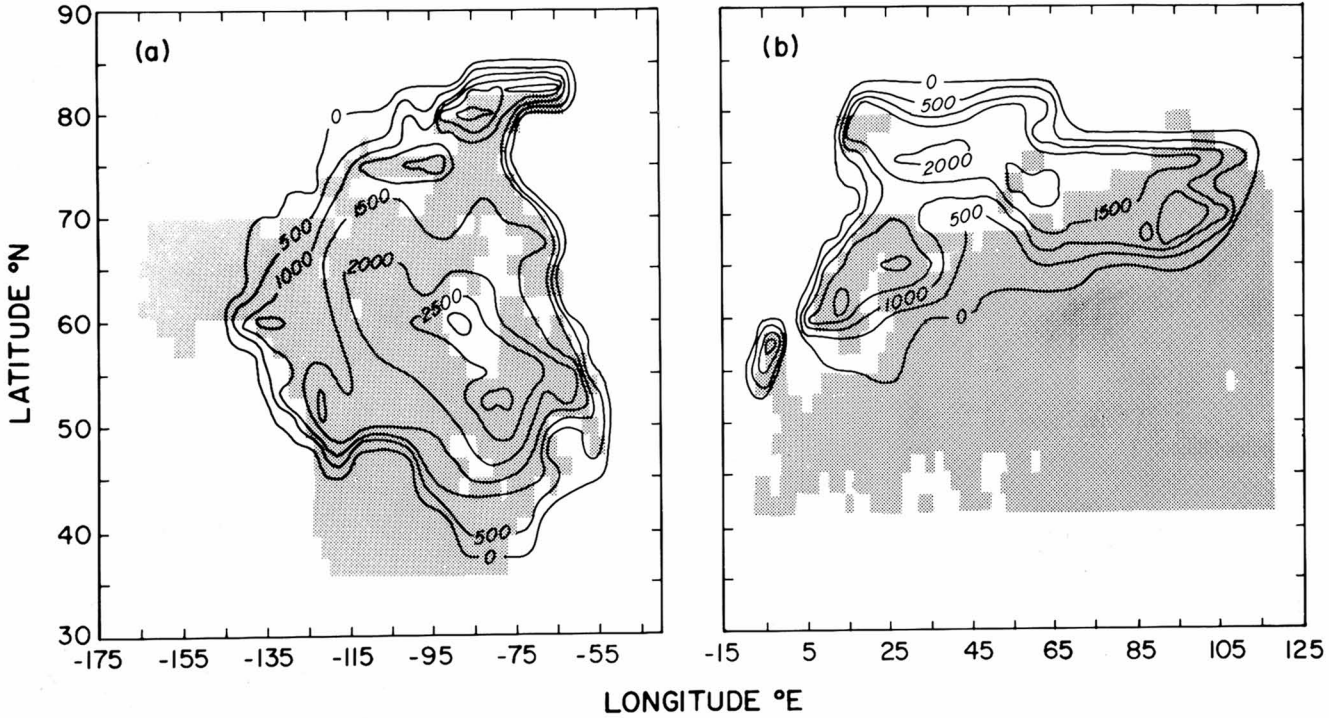

Figure 9. Thickness isopleths for the North American (a) and Fennoscandian (b) ice complexes at last glacial maximum according to the deconvolution of post glacial relative sea level records by Tushingham and Peltier (1991).

satisfactory explanation of the origins of the termination process.

In this more realistic model the same evolution equation for ice thickness is employed as previously and glacial isostatic adjustment is also explicitly described, though both of these processes are taken to be both longitude and latitude dependent rather than latitude dependent only. The main enhancement of the dynamical system consists of the explicit solution for the longitude and latitude dependence of the annual cycle of the sea level temperature field through the integration of the following energy balance equation:

$$C(\underline{r})\,\frac{\partial T(\underline{r},t)}{\partial t} - \underline{\nabla}_h \cdot \left[D(x)\,\underline{\nabla}_h T(\underline{r},t)\right] + A + BT(\underline{r},t) = \frac{Q}{4}\,a(\underline{r})\,S(x,t) \qquad (7)$$

in which $C(\underline{r})$ is the effective heat capacity (equal to C_l over land, C_w over water and C_i over sea ice), D(x) is a diffusion coefficient intended to represent all forms of heat transport (baroclinic eddies etc.), A+BT represents the longwave emission to space with the empirical coefficients A and B determined by fitting to modern satellite data, Q = 1360 W/m^2 is the solar constant and $a(\underline{r})$ is the coalbedo (the fraction of the solar energy per unit area and time that is absorbed by the earth) and S(x,t) is the solar distribution function. With D expanded to degree 4 in Legendre polynomials the linear energy balance model embodied in (7) is essentially that of North et al. (1983). It is linear in the sense that $a(\underline{r})$ is not a function of T and so, for example, sea ice extent cannot be carried as a prognostic variable.

The ice sheet model to which this linear energy balance model is linked is essentially a two-dimensional version of (1) and takes the form:

$$\frac{\partial H}{\partial t} = \underline{\nabla}_h \cdot (D_i\,\underline{\nabla}_h h) + G(\theta,\phi,t) \qquad (8)$$

in which the highly nonlinear diffusion coefficient is just:

$$D_i = B_1\,H^{m+1}\,(\underline{\nabla}_h h \cdot \underline{\nabla}_h h)^{\frac{(m-1)}{2}}$$

with $B_1 = \lambda(\rho_i g)^m$ and the stress-exponent $m \sim 3$ based upon experimental observations of ice rheology. The dependent variables H, h, and G are as previously. Now in two spatial dimensions the accurate model of glacial isostatic adjustment embodied in (3) is quite numerically demanding to integrate and I have therefore elected to replace it for the purpose of

initial experiments with the simpler local adjustment model embodied in the equation:

$$\frac{\partial h'}{\partial t} = -\frac{(h' - h_o')}{\tau} + \left(\frac{\rho_i}{\rho_e \tau}\right) H \qquad (9)$$

in which $h' = H-h$ is the depth of the bedrock measured positive below a given reference level, ρ_e is the density of the bedrock and h_o' is the bedrock depression which is assumed to be in isostatic balance in the absence of a load, essentially the present day topography relative to mean sea level. τ is the isostatic adjustment timescale.

Now the critical part of the above described model concerns the manner in which the ice sheet and energy balance components are coupled together and this is taken to occur through the mass balance function $G(\theta,\phi,t)$. This function is taken to consist of two parts, an accumulation function defined as

$$\begin{aligned} G_c\,(m/month) &= P(\theta,\phi)\, L_m, \; T_c(\theta,\phi) \le 0 \\ &= 0 \qquad\qquad , \; T_c(\theta,\phi) > 0 \end{aligned} \qquad (10)$$

in which the T_c are now monthly average values of the temperature determined by solving (7) for the "instantaneous" annual cycle and corrected for height, $P(\theta,\phi)$ in m/yr is the present day annually averaged precipitation and L_m is the duration of a month. The accumulation function in (10) is further adjusted for the so-called elevation desert effect by correcting it to:

$$G_{cc} = G_c \; x \; (2^{-max(o,[h(km)-2])}) \,, \qquad (11)$$

following Budd and Smith (1981). To obtain the net mass balance at every surface point in the model we next compute an ablation function in the form:

$$G_g(m/month) = max(0, aT_c(^{\circ}C) + bR_m(W/m^2) + c) \cdot (10/\rho_i[km/m^2]) \qquad (12)$$

In this expression the field $T_c\,(\theta,\phi)$ is the same as previously while R_m is the monthly mean insolation at the top of the atmosphere. The parameters a,b,c have been obtained by fitting present day ablation rates on glaciers (e.g. Pollard 1983).

With all parameters of the model now specified it can be directly integrated to simulate the evolution of the space-time distribution of ice from the last interglacial (Eemian) period to the present, with R_m (θ,t) being determined by the orbital variations. The model is in fact run in "a-synchronous" mode, beginning with the construction of an equilibrium annual cycle by solution of (7). The ice sheet and bedrock adjustment equations are next integrated forward for 1000 years of model time, during which the annual cycle is assumed to be stationary. A new equilibrium annual cycle is next calculated using the updated surface ice distribution to modify the albedo function and the new annual cycle is again held stationary while the ice sheet and bedrock equations are again integrated forward for 1000 years. The optimum time step separating recomputations of the annual cycle has been determined by numerical experimentation to be the longest compatible with a sufficiently accurate prediction of the history of ice sheet evolution.

A typical example of a prediction of the distribution of surface ice at LGM based upon this model (after DeBlonde and Peltier 1991b) is shown on Figure 10. Comparing this distribution with that previously inferred by Tushingham and Peltier on the basis of the inversion of relative sea level histories (Figure 9) it is clear both on the basis of the geographical location of the continental ice sheets and on the basis of their maximum thicknesses that the above described model rather accurately describes these aspects of the LGM ice cover. The reasons for the success of the model are also quite easily understood. Laurentian ice is prevented from invading the American sector of the North American continent by the latitudinal insolation gradient which drives ablation rates to extremely high levels south of about 45°N latitude. Similarly the Fennoscandian ice sheet is inhibited from expanding eastward by the extremely large amplitude of the annual cycle that obtains in the interior of the vast Eurasian continent. Summers there are simply too warm to permit perennial snow cover to develop. The remaining fractions of the perimeters of Laurentian and Fennoscandian ice are coincident with the continental shelves, beyond which water depth increases rapidly leading to extremely high calving rates and confinement of the ice sheets to their proximate continents.

Although the above described successes of the energy balance coupled ice sheet model described in this section must be seen as encouraging there are also aspects of the model integration, discussed more fully than is possible here in DeBlonde and Peltier (1991b), that are considerably less than satisfactory. In particular the present model suffers the same flaw as was

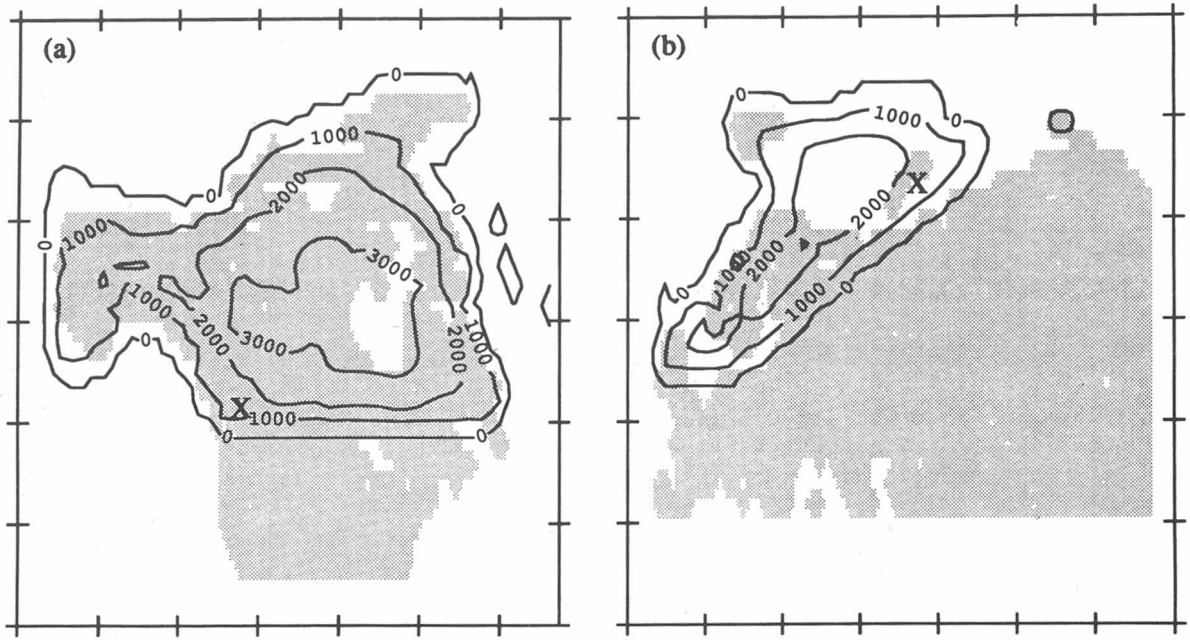

Figure 10. Ice thickness at glacial maximum for the Laurentian (a) and Fennoscandian (b) regions predicted by the ice sheet coupled energy balance model described in the text. These plates should be compared with the "observed" distributions shown on Figure 9.

revealed by the integrations of the one-dimensional analogous model discussed in the last Section. This concerns the inability of the model to properly explain the termination process. Although ice volume does diminish significantly following LGM in response to the orbital forcing alone, this diminution is insufficient to explain the observed Holocene distribution of land ice. Although the use of a nonlinear version of the energy balance model embodied in (7), as discussed in DeBlonde et al. (1992), can somewhat improve this critical aspect of the simulation, especially if representations are included in the model of the additional forcing associated with CO_2 variations and heat flux effects associated with changes in the strength of the thermohaline circulation (DeBlonde and Peltier 1993) the complete collapse of the Laurentide ice sheet still proves difficult to understand. Additional feedbacks, either "wet" or "dry", still appear to be required to understand the near complete deglaciations of Canada and Fennoscandia that occurred. What these additional required feedbacks might be is addressed in the following Section.

Conclusions

The results discussed in the previous sections of this paper illustrate a number of recent advances that have been achieved in our understanding of the 100 kyr ice age cycle that has dominated climate system variability for the last 900 kyr of earth history. The chronology of ice volume changes through the full Pleistocene epoch is now rather well determined by the advanced tuning strategy discussed above that has been so successfully applied to the ODP 677 core from the Panama Basin. This record shows that the 100 kyr oscillation "turned-on" smoothly in the time interval from 900 kyr BP to about 700 kyr BP. Prior to 900 kyr BP the variance in the ice volume record was contained almost entirely in the orbitally related spectral peaks corresponding to the periods 41 kyr, 23 kyr, 21 kyr and 19 kyr. Such variability is just as expected on the basis of the Milankovitch hypothesis with ice volume linearly related to the summertime (caloric) seasonal insolation anomaly. Subsequent to this mid-Pleistocene climate transition the 100 kyr cycle has dominated the records of $\delta^{18}0$ change. This cycle is not expected on the basis of the Milankovitch hypothesis which is therefore not in detailed accord with observations.

In order to understand the origins of the 100 kyr cycle one is obliged to introduce an appropriate nonlinearity into the physical model of climate system behaviour that governs the response on the very long timescales of the evolution of the planetary orbit. Analysis of a simple

1-D model that couples the nonlinear physics of the accumulation and flow of a continental ice sheet with the physics of glacial isostatic adjustment demonstrates that a large fraction of the variability in ice volume may be thereby explained but strong 100 kyr oscillations only appear when an additional feedback loop is added to the model such that meltback is enhanced when it exceeds some critical threshold. This model provides no means whereby the precise origins of the required feedback may be assessed, however, making the model less satisfactory than one might hope.

Increasing the precision with which the ice physics and accumulation processes are described, especially when the energy balance model to which the ice sheets are linked is made nonlinear, does improve the quality of the "terminations" delivered by the climate model somewhat though not sufficiently to allow us to claim that the model provides a good fit to the data. As discussed in the last section of this paper, even adding explicit descriptions of the "known" feedbacks associated with variations in the concentration of CO_2 and with the strength of the North Atlantic heat pump that is linked to the strength of the thermohaline circulation fail to explain, in the non-linear energy balance context, the near complete "termination" of the Laurentide ice sheet that marked the onset of Holocene time.

In my view there remain two excellent candidates for the remaining feedback needed to induce total deglaciation of the dominant Laurentian ice mass. The first of these, a "dry" mechanism, involves the feedback onto surface albedo that is expected to be caused by the marked increase of terrigenous dust load in the atmosphere that was apparently characteristic (DeAngelis et al., 1988) of the time of glacial maximum, not only of the last glacial maximum recorded in ice cores but also of previous glacial maxima as recorded in deep sea sedimentary cores. This increase in terrigenous dust load is always observed to precede the termination and could constitute the missing feedback as recently argued in the analyses described by Peltier and Marshall (1993). A possible wet mechanism that could be competitive, in my view, with this dry mechanism might consist of a marine instability of the Laurentide ice sheet, perhaps the same instability, now aided by insolation forcing, that is presumably responsible for the so-called Heinrich events (Heinrich, 1988) that have recently been identified in deep sea cores from the North Atlantic basin and which appear to record, in the quasi-cyclic appearance of ice rafted debri, occasions of intense instability of the eastern flank of the Laurentide ice sheet during the time of maximum ice cover. Which of these two equally plausible feedback loops is principally

responsible for the disappearance of Laurentide ice is as yet unclear but prospects are rather good that further application of the model based strategy described here, for inferring what the observations can be taken to imply, can be expected to lead to a deepening of understanding.

References

Baksi, A.K., V. Hsu, M.O. McWilliams and E. Farrar, 1992, $^{40}Ar/^{39}Ar$ dating of the Brunhes-Matuyama geomagnetic field reversal. *Science*, **256**, 356-34.

Berger, A., 1978, Long term variations of calorific insolation from the Earth's orbital elements. *Quat. Res.*, **9**, 139-167.

Broecker, W.S. and J. Van Donk, 1970, Insolation changes, ice volumes and the $\delta^{18}0$ record in deep sea cores. *Rev. Geophys. Space Phys.*, **8**, 169-198.

Broecker, W.S. and G.H. Denton, 1989, The role of ocean-atmosphere reorganizations in glacial cycles. *Geochim. Cosmochim. Acta.*, **53**, 2465-2501.

Budd, W.F. and I.N. Smith, 1981, The growth and retreat of ice sheets in response to orbital radiation changes, sea level, Ice and Climate Changes, IAHS Publ. **131**, 369-409.

Cox, Allan, R.R. Doell and G.B. Dalrymple, 1963, Geomagnetic polarity epochs and Pleistocene geochronometry. *Nature*, **198**, 1049-1051.

De Angelis, M., N.I. Baskov and V.N. Petrov, 1987, Aerosol concentrations over the last climatic cycle (160 kyr) from an Antarctic ice core. *Nature*, **325**, 318-321.

DeBlonde, G. and W.R. Peltier, 1991a, A one dimensional model of continental ice volume fluctuations through the Pleistocene: Implications for the origin of the mid-Pleistocene climate transition. *J. Climate*, **4**, 318-344.

DeBlonde, G. and W.R. Peltier, 1991b, Simulations of continental ice sheet growth over the last glacial-interglacial cycle: experiments with a one-level seasonal energy balance model including realistic geography. *J. Geophys. Res.*, **96**, 9189-9215.

DeBlonde, G., W.R. Peltier and W.T. Hyde, 1992, Simulations of continental ice sheet growth over the last glacial-interglacial cycle: experiments with a one level seasonal energy balance model including seasonal ice-albedo feedback. *Global and Planetary Change*, **98**, 37-55.

DeBlonde, G. and W.R. Peltier, 1993, Late Pleistocene ice age scenarios based upon observational evidence. *J. Climate*, **6**, 709-727.

Hays, J.D., J. Imbrie and N.J. Shackleton, 1976, Variations in the Earth's orbit: pacemaker of the ice ages. *Science*, **194**, 1121-1132.

Heinrich, H., 1988, Origin and consequences of cyclic ice rafting in the Northeast Atlantic Ocean during the past 130,000 years. *Quat. Res.*, **29**, 142-152.

Hyde, W.T. and W.R. Peltier, 1985, Sensitivity experiments with a model of the ice-age cycle: the response to harmonic forcing. *J. Atmos. Sci.*, **42**, 2170-2188.

Hyde, W.T. and W.R. Peltier, 1987, Sensitivity experiments with a model of the ice-age cycle: the response to Milankovitch forcing. *J. Atmos. Sci.*, **44**, 1351-1374.

Imbrie, J., N.J. Shackleton, N.G. Pisias, J.J. Morley, W.L. Prell, D.G. Martinson, J.D. Hays, A. McIntyre and A.C. Mix, 1984, The orbital theory of Pleistocene climate: support from a revised chronology of the marine $\delta^{18}0$ record. In *Milankovitch and Climate*, A. Berger and coeds., 269-305.

Martinsen, D.G., N. Pisias, J.D. Hays, J. Imbrie, T.C. Moore and N.J. Shackleton, 1987, Age dating and orbital theory of the ice ages: development of a high resolution 0-300,000 - year chronostratigraphy. *Quat. Res.*, **27**, 1-30.

Milankovitch, M., 1941, Canon of insolation and the ice age problem, and glacial cycles, K. Serb. Acad. Beorg. Spec. Publ. 132.

North, G.R., J.R. Mengel and D.A. Short, 1983, Simple energy balance model resolving the seasons and the continents: Application to the astronomical theory of the ice ages. *J. Geophys. Res.*, **88**, 6576-6586.

Oerlemans, J., 1980, Model experiments on the 100,000 year glacial cycle. *Nature*, **287**, 430-432.

Peltier, W.R., 1974, The impulse response of a Maxwell earth. *Rev. Geophys. and Space Phys.*, **12**, 649-669.

Peltier, W.R., 1976, Glacial isostatic adjustment II. The inverse problem. *Geophys. J.R. astron. Soc.*, **46**, 669-706.

Peltier, W.R, 1982, Dynamics of the ice age earth. *Adv. Geophys.*, **24**, 1-146.

*Peltier, W.R., 1985, The LAGEOS constraint on deep mantle viscosity: results from anew normal mode method for the inversion of viscoelastic relaxation spectra. *J. Geophys. Res.*, **90**, 9411-9421.

*Peltier, W.R. and S. Marshall, 1993, Glacial terminations and terrigenous dust: experiments with

a nonlinear ice sheet coupled energy balance model, J. Climate, submitted.

Pollard, D., 1982, A simple ice sheet model yields realistic 100 kyr glacial cycles. *Nature*, **296**, 334-338.

Pollard, D., 1983, A coupled climate - ice sheet model applied to the Quaternary ice ages. *J. Geophys. Res.*, **88**, 7705-7718.

Quinn, T.R., S. Tremaine and M. Duncan, 1991, A 3 million year integration of the Earth's Orbit. *Astronomical Journal*, **101**, 2287-2305.

Raymo, M.E., W.F. Ruddiman, N.J. Shackleton and D.W. Oppo, 1990, Evolution of global ice volume and Atlantic-Pacific $\delta^{13}C$ gradients over the last 2.5 M.Y. *Earth and Planet. Science Lett.*, **97**, 353-368.

Shackleton, N.J. 1967, Oxygen isotope analysis and Pleistocene temperatures readdressed. *Nature*, **215**, 15-17.

Shackleton, N.J. and M.A. Hall, 1989, Stable isotope history of the Pleistocene at ODP Site 677. K. Becker, H. Sakai et al., Eds., Proc. ODP Sci. Results, **3**, College Station, Tx.

Shackleton, N.J., A. Berger and W.R. Peltier, 1990, An alternative astronomical calibration of the lower Pleistocene timescale based upon ODP Site 677. *Trans. Roy. Soc. Edinburgh; Earth Sciences*, **81**, 251-261.

Tushingham, M. and W.R. Peltier, 1991, ICE-3G: A new global model of late Pleistocene deglaciation based upon geophysical predictions of post-glacial relative sea level change. *J. Geophys. Res.*, **96**, 4497-4523.